

Combustion of biomass pyrolysis gas: Roles of radiation reabsorption and water content

Shu Zheng^a, Hao Liu^a, Yuzhen He^a, Yu Yang^a, Ran Sui^{b, **}, Qiang Lu^{a,*}

^a National Engineering Research Center of New Energy Power Generation, North China Electric Power University, Beijing, 102206, China

^b Center for Combustion Energy, Department of Energy and Power Engineering, Tsinghua University, Beijing, 100084, China



ARTICLE INFO

Keywords:

Biomass pyrolysis gas
H₂O content in py-gas
Radiation reabsorption
Laminar flame speed
NO emission

ABSTRACT

Biomass energy has drawn increased attention owing to its zero carbon emissions and large reserves. Pyrolysis instead of direct combustion is an efficient and clean way for biomass energy conversion. As a strong radiative species, H₂O greatly affects the combustion processes. Despite the large concentration and fluctuation of H₂O content in biomass pyrolysis gases (py-gas), radiation reabsorption effect has not been systematically investigated for py-gas combustion. In this study, one-dimensional simulations of premixed py-gas/air flames were conducted, using PREMIX code with both adiabatic and radiative models. The effects of H₂O content and radiation reabsorption were examined. As H₂O content in the py-gas mixture increased from 40% to 50%, the flame speeds decreased from 42.86 to 28.08 cm/s, while the relative differences caused by radiation reabsorption increased from 9.92% to 17.42%. Radiation reabsorption affected laminar flame speed primarily through the preheat-induced chemical effect, which was mainly controlled by HCO radical. The outlet mole fraction of NO was reduced by up to 13.56% when radiation reabsorption was considered. Reaction pathway analyses revealed that the NO emission was closely related to the outlet temperature and the peak NCO concentration, which were the limiting factors for the thermal-NO route and the fuel-NO route, respectively.

1. Introduction

With the deterioration of environment and shortage of energy, it is necessary to reduce the consumption of fossil fuels and use renewable energy more efficiently. Biomass is a promising renewable energy resource with zero carbon emissions, large reserves and wide availability [1]. Direct combustion is the most common method for biomass utilization, which easily converts biochemical energy into thermal energy and power with a low cost [2]. However, because of the low heating values, large non-combustible impurities and high moisture content of biomass raw materials, there are many issues with the direct biomass combustion, such as incomplete burning that leads to a large amount of slag. The past studies by Morris et al. [3] and Cruz et al. [4] manifested that biomass requires substantial preprocessing before its direct combustion. Among the preprocessing methods, pyrolysis is recognized as an excellent choice for efficient and clean energy conversion. The combustion of biomass pyrolysis gas (py-gas), namely the pyrolysis-generated volatiles composed of non-condensable gases and condensable bio-oils [5], not only reduces NO emission effectively [6]

but also provides more efficient energy conversion for renewable energy utilization.

The compositions of py-gases are rather complex [7], especially the condensable bio-oils, which consist of water and more than 300 highly oxygenated compounds [8]. Of special importance is the varying water content, which is the most abundant component of bio-oils (typically 15–35 wt%) and has a significant effect on the combustion stability and pollutant emissions [9]. Hence, the water contents adopted in previous studies were also quite different: The initial water content in spruce wood chips used by Burhenne et al. [10] varied from 2.4% to 55.4% by weight, while the pine wood used as feedstock by Westerhof et al. [11] had moisture contents between 0 and 20 wt%. The study of classification and composition of biomass conducted by Tumuluru et al. [12] indicated that fresh wood typically contained more than 50% water, and the high water content reduced the flame temperature and increased the necessary residence time, consequently resulting in incomplete combustion and increased pollutant emission. To further investigate the effect of water content in non-condensable pyrolysis gas, Meng et al. [13] studied the laminar flame speeds of CO/H₂/O₂/H₂O mixtures with

* Corresponding author.

** Corresponding author.

E-mail addresses: sui@tsinghua.edu.cn (R. Sui), qianglu@mail.ustc.edu.cn (Q. Lu).

0–60% water content, demonstrating that the water content affected laminar flame speed through both thermal properties and chemical kinetics, which thus had a significant impact on combustion. Anufriev [14] examined the chemical and physical reduction effects of water/steam on NO_x, with the former primarily related to the OH concentration and the latter mainly reduced thermal NO_x by affecting the flame temperature. Munajat et al. [15] studied the influence of water vapor on the laminar flame speed of gasified biogases (components including CO, CO₂, CH₄, H₂O and C₆H₆, etc.), and the results indicated that decrease of flame speed occurred with water addition. However, this study did not take into account the chemical and radiation effects of H₂O addition on the combustion process, nor did they pay attention to the impact on pollutant emission. In summary, although the important role of water content has been shown by the above studies, systematic studies on the effects of water content during py-gas combustion have not been conducted.

Furthermore, several previous studies have highlighted the radiation effect of the strong radiative species such as H₂O, CO₂ and CO on flame parameters. Sohn et al. [16] investigated the laminar flame speeds of CH₄/air and H₂/air flames with CO₂/H₂O/CO dilutions. Results showed that radiation could cause a large uncertainty in the determination of flame speed. Yoshinaga et al. [17] emphasized the radiative effect of H₂O in polypropylene combustion. They observed the chemical and radiative effects in the temperature profiles, and suggested that the radiative effect of H₂O greatly enhanced the regression rate. Wang et al. [18] investigated the radiation reabsorption effects on NO_x formation in CH₄ flames, and found that the impact of radiation reabsorption on NO formation was significantly strengthened with addition of the strong absorber CO₂. Despite the above literature studies on fundamental fuels, such investigations have not been conducted for biomass related combustion. Because of the high contents of CO, CO₂ and H₂O in biomass py-gas, their radiation reabsorption effect is expected to have a strong impact on the combustion characteristics and hence should be taken into consideration when simulating py-gas combustion.

In view of energy conversion efficiency and pollutant emission during biomass py-gas combustion, the laminar flame speed and NO emission were numerically calculated with the consideration of radiation reabsorption in this study. Subsequently, the dependence of flame speed and NO emission on H₂O content was discussed and explained. Finally, the detailed mechanism of radiation reabsorption effects with various H₂O contents on py-gas combustion was elaborated via ROP (rate of production) and sensitivity analyses.

2. Computational details

2.1. Surrogate model of biomass pyrolysis gas

As mentioned above, considering the complex and varying compositions, it is difficult to take all the components of actual py-gas into account during numerical simulations. Thus, as listed in Table 1, representative components were adopted in the surrogate model based on the following considerations: The yield ratio of non-condensable gas and condensable bio-oil was set as 2:5 based on previous study [19]. The

non-condensable gas is consisted of CO₂, CO and CH₄, which accounted for the majority of typical pyrolysis gases, and their proportions were set as 6:3:1 based on the product distribution from pyrolysis of wood [19]. In terms of the condensable bio-oil, H₂O is the most abundant component, processing a high content of 30 wt% [20]. The other complex compounds in bio-oils were simplified according to the isomerism relationships. Acetic acid (CH₃COOH) was selected as the representative of acids and esters, ethanol (CH₃CH₂OH) for alcohols and ethers, and aldehydes and ketones were substituted by furfural (C₄H₅OCHO). The content of phenols (and other aromatic compounds) was considered by including phenol (C₆H₅OH). Finally, as the predominant nitrogen-containing species in biomass pyrolysis products [21], pyridine was included in the simulations to investigate the formation of fuel-NO_x. The contents of the compounds mentioned above were determined based on the references [22–25].

2.2. Settings of numerical simulation

To investigate the impact of H₂O content on the combustion performance, mole fraction of H₂O was altered in the range of 40–50%, and all the other components in the py-gas were scaled accordingly. The py-gas was subsequently premixed with air and the air-fuel ratio was set as 6:1 by volume (the corresponding equivalence ratio φ ranged from 0.89 to 0.74 as H₂O content altering from 40% to 50%), with the inlet temperature $T_{in} = 400$ K at atmospheric pressure, according to actual industrial applications. To take radiation reabsorption effects into consideration, two computational models were used in the numerical simulations: the adiabatic model (ADI) and the statistical narrow-band model (SNB). The ADI model is an adiabatic model without radiation, while the SNB model can comprehensively calculate the radiative heat loss outside the flame and the heat transfer in the flame with good accuracy and efficiency [26,27]. Comparisons between the two computational models thus reflected the effect of radiation reabsorption. In the SNB model, the radiative parameters of H₂O, CO₂ and CO were calculated based on the HITRAN 2016 database [28]. Narrow band average spectral line strength $\bar{\kappa}_\eta$, narrow band average spectral line half band-width $\bar{\gamma}_\eta$ and the narrow band average spectral line interval $\bar{\delta}_\eta$ were used to obtain the narrow band averaged transmissivity $\bar{\tau}_\eta(L)$ [29]. Subsequently, the radiative transfer equation (RTE) was solved by the discrete ordinate method (DOM) and the net radiative flux was obtained.

One-dimensional simulations of steady laminar py-gas/air flames were conducted using the PREMIX package of CHEMKIN [30], with a computational domain ranging from $x = -10$ cm at the upstream to $x = 20$ cm at the downstream. A detailed chemical kinetic mechanism of 145 species and 1301 reactions was combined from several literatures to cover all the simulated biomass py-gas species. Considering the highest concentration of CH₃COOH among the bio-oil fuel species, the Christensen model [31] developed for CH₃COOH combustion was selected as the base mechanism, which included detailed oxidation mechanism of C₀–C₃ species [32]. Reactions of furfural and phenol that depicted their decomposition processes to C₃ species derived from Jin's [33] and Pelucchi's models [34], respectively, were incorporated into the present model. The detailed mechanism NOMEcha 2.0 [35] and Wu's pyridine mechanism [36] were also added to account for the NO emission, which were both validated by high temperature experiments under fuel-lean conditions. The detailed mechanism is attached in the supplementary material.

To verify the accuracy of the mechanism adopted in this work, laminar flame speeds of the main components in the biomass py-gas model as well as NO formation were compared against experimental results in the literature. As shown in Fig. 1(a), the predictions were in good agreement with the measurements of CH₄ [37], C₅H₆ [38] (an important intermediate during the oxidation of phenol), CH₃CH₂OH [39] and CH₃COOH [40], with the initial temperature ranging from 300 K to 423 K. As for minor species such as NO, HCN and N₂O, the adopted

Table 1
Model component composition in biomass py-gas.

	Component	mass fraction (%)	mole fraction (%)
non-condensable gas	CO ₂	17.14	13.80
	CO	8.57	10.84
	CH ₄	2.86	6.33
condensable bio-oil	H ₂ O	21.43	42.17
	CH ₃ COOH	17.86	10.54
	CH ₃ CH ₂ OH	10.71	8.25
	C ₄ H ₅ OCHO	14.29	5.27
	C ₆ H ₅ OH	5.71	2.15
	C ₅ H ₅ N	1.43	0.64

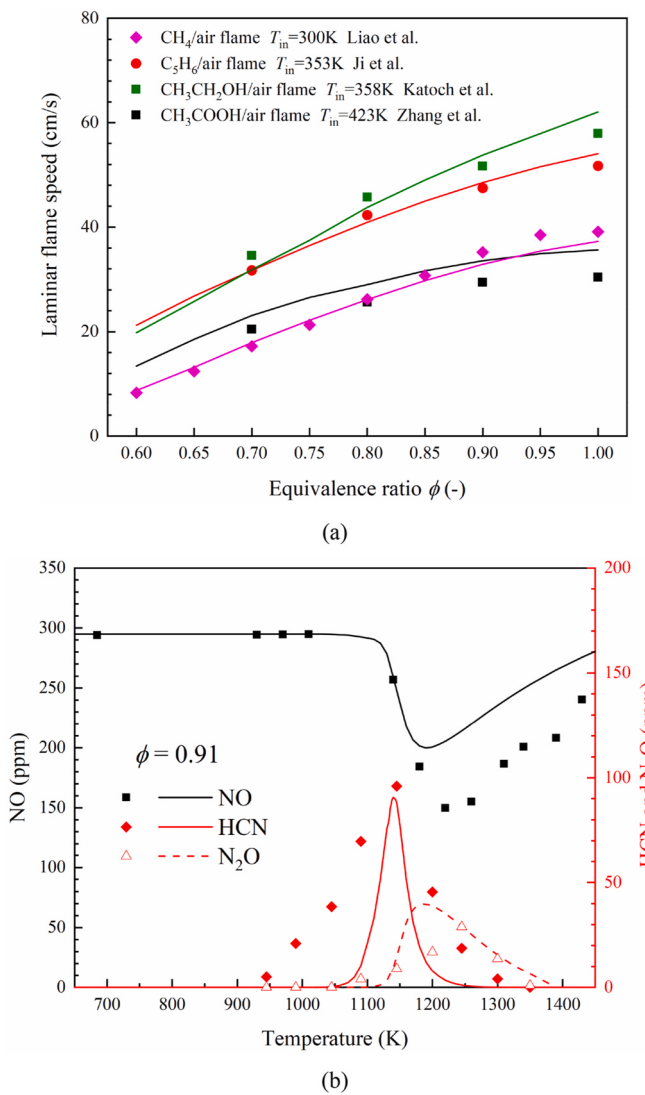


Fig. 1. Comparison of experimental data (samples) and predictions (lines) for (a) laminar flame speeds of main fuel components in the biomass py-gas as a function of equivalence ratio and (b) outlet mole fractions of NO and HCN as a function of temperature.

mechanism also well reproduced their measurements from pyrrole (111 ppm) oxidation [41] as a function of temperature in Fig. 1(b).

3. Results and discussion

3.1. Effects on flame speeds

Fig. 2 shows the laminar flame speeds of py-gas/air flames calculated using ADI and SNB models with various H_2O contents and a fixed inlet temperature $T_{in} = 400\text{ K}$ at atmospheric pressure. On the one hand, the laminar flame speeds calculated with ADI and SNB both decreased with rising H_2O content, indicating that the increased H_2O fraction inhibited the combustion of py-gas. On the other hand, the flame speeds calculated by SNB were consistently higher than those by ADI, originating from the radiation reabsorption effect that preheated the cold unburned upstream mixture and thereby facilitated the reactions. The relative differences of laminar flame speeds R_s , quantified as $(S_{L,\text{SNB}} - S_{L,\text{ADI}})/S_{L,\text{ADI}}$, between the two models increased from 9.92% to 17.42% when the H_2O content in the py-gas was increased from 40% to 50%, reflecting the radiation reabsorption effect was accentuated by the increased H_2O content.

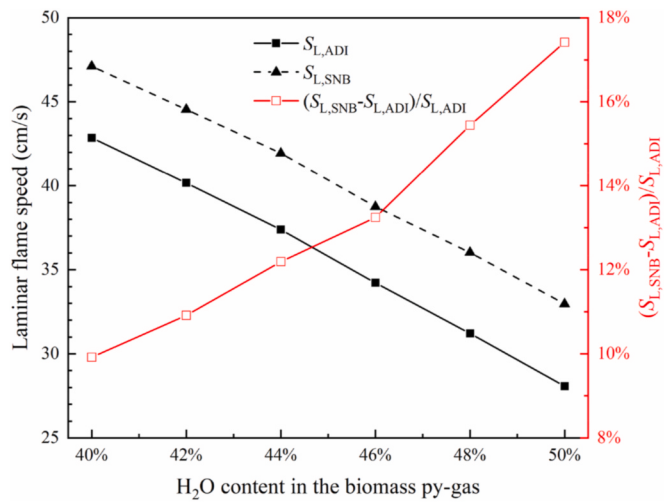


Fig. 2. Laminar flame speeds calculated by ADI and SNB models and the effect of radiation reabsorption on laminar flame speed for py-gas/air mixtures with various H_2O contents ($P = 1\text{ atm}$ and $T_{in} = 400\text{ K}$).

To explore how H_2O content affected the flame structures of py-gas/air flames, 1D distributions of temperature, major species (H_2O , CO and CH_3COOH) and important radicals (H, OH, O and HCO) around the flame surface are shown in Fig. 3, calculated by ADI with two H_2O contents (40% and 50% vol. in the py-gas). Obviously, the flame temperature was reduced when more H_2O was added due to its role as a diluter and heat adsorber. As a result, the depletion of fuels (CH_3COOH and CO) and the generation of H_2O slowed down (see the less steep dashed lines for CH_3COOH , H_2O and the delayed peak value for CO). Besides dilutive and thermal effects, increased H_2O content also affected the combustion process through radical concentrations [13], i.e., chemical effect. As shown in Fig. 3 of the mole fractions of important radicals, OH, the primary radical generated through the decomposition

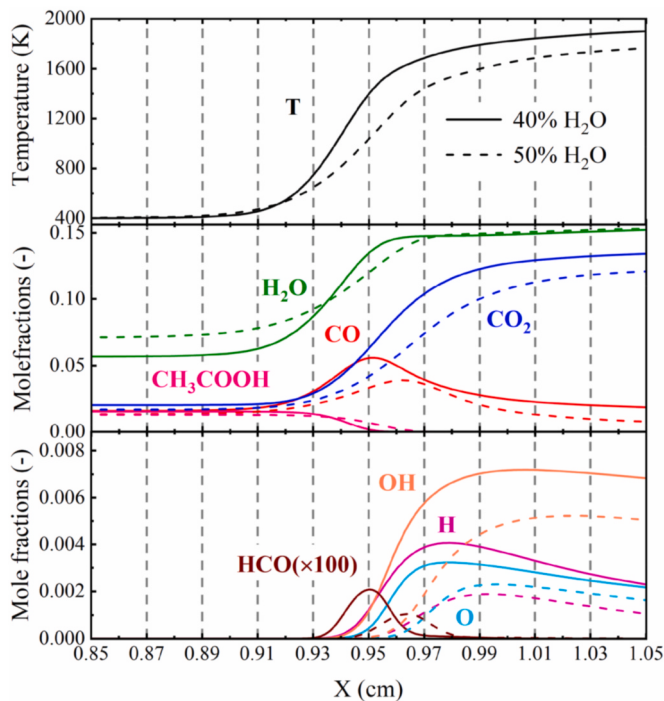


Fig. 3. Distributions of temperature, major species and important radicals for py-gas/air mixtures with two H_2O contents (solid: 40%; dashed: 50% in the py-gas).

of CH_3COOH , had higher mole fraction than H and O. The peak mole fractions of H, OH, O and HCO radicals all dropped and were postponed when H_2O content was higher in the inlet, a behavior similar to the dependence of flame speed on H_2O .

To gain a better understanding on how the chemical effect of varying H_2O content influenced the combustion characteristics of py-gas/air mixtures, sensitivity analysis of flame speed was conducted for three H_2O contents (40%, 44% and 50% vol. in the py-gas). The most sensitive reactions affecting flame speed are shown in Fig. 4. It is noted that the positively sensitive reactions with maximum sensitivity coefficients, $\text{CO} + \text{OH} = \text{CO}_2 + \text{H}$ and $\text{H} + \text{O}_2 = \text{OH} + \text{O}$, were both concerned with H and OH radicals, which are more active and abundant than other radicals. Plenty of investigations on burning velocity of hydrocarbon or hydrogen-containing fuels [42,43] also concluded that the laminar flame speed was closely relevant to the maximum mole fractions of H and OH radicals. Besides, HCO radical, which was the main radical decomposed from the larger molecules in bio-oil, also played an important role as it was concerned with nearly half of the top sensitive reactions, including the most negatively sensitive reaction $\text{HCO} + \text{O}_2 = \text{CO} + \text{HO}_2$. HCO was mainly derived from furfural $2\text{OH}_3\text{J}$ and CH_2O . The former originated from the decomposition of furfural, while the precursor of the latter, CH_2OH , was closely associated with $\text{CH}_3\text{CH}_2\text{OH}$ (via the reaction $\text{C}_2\text{H}_5\text{OH} = \text{CH}_2\text{OH} + \text{CH}_3$) and CH_3COOH (via the intermediate CH_2CO).

Furthermore, ROP analyses were conducted for H_2O to clarify its impact on H/OH radicals, whose peak concentrations were strongly correlated with the flame speed. As shown in Fig. 5(a), the ROP results for the (reverse) reaction $2\text{OH} = \text{H}_2\text{O} + \text{O}$, i.e., the main pathway that consumed H_2O , increased with the enhancing H_2O content, indicating that it consumed more O radical as the H_2O content increased. Additionally, the ROP results for the important chain termination reaction $\text{HO}_2 + \text{OH} = \text{H}_2\text{O} + \text{O}_2$ increased significantly with the rising H_2O content despite H_2O was a product of this reaction, and consumed the OH radical. Moreover, the ROPs of this reaction increased much more drastically than those of reversed $2\text{OH} = \text{H}_2\text{O} + \text{O}$ when more H_2O was added in the fuel, and this explains why OH was significantly reduced (as shown in Fig. 3) when more H_2O was added in the py-gas.

The ROP results for O radical in Fig. 5(b) further manifested that more O radical were consumed through reversed $2\text{OH} = \text{H}_2\text{O} + \text{O}$ when H_2O content was increased. The ROP results for other reactions that consumed O (which generated H and OH) were suppressed, such as the chain branching reaction $\text{O} + \text{H}_2 = \text{OH} + \text{H}$. Therefore, the increase of H_2O content consumed more O radical and led to the decrease of H and OH in the radical pool.

Next, to explore the role of radiation reabsorption on flame speed, the direct radiative effect, which was determined by optical thickness and absorption coefficient, is discussed. The principle of the calculation formula of optical thickness was detailed in Ref. [44] and the absorption coefficient was represented by the mole fractions of the strongly radiating species (i.e., the total mole fraction of CO_2 , H_2O and CO) in the

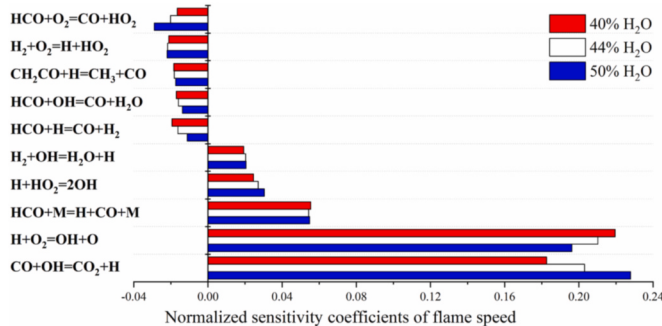
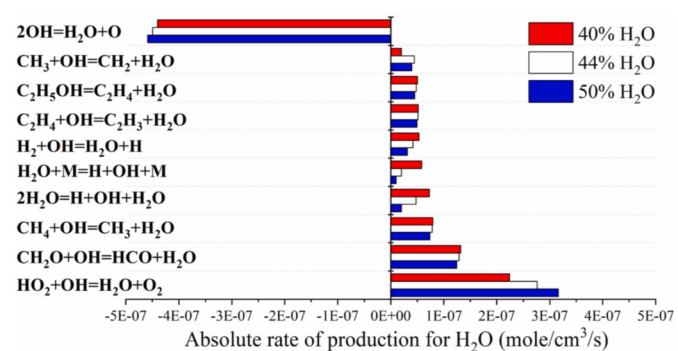
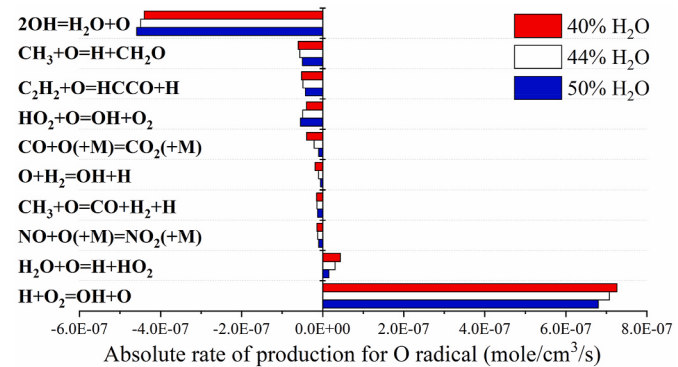


Fig. 4. Normalized sensitivity coefficients of laminar flame speed for py-gas/air mixtures with various H_2O contents ($P = 1$ atm and $T_{\text{in}} = 400$ K).



(a)



(b)

Fig. 5. Rates of production of (a) H_2O and (b) O radical for py-gas/air mixtures with various H_2O contents ($P = 1$ atm and $T_{\text{in}} = 400$ K).

upstream unburned region. As shown in Fig. 6, the optical thickness that blocked radiative heat transfer within the flame increased with the rising H_2O content. Meanwhile, the absorption coefficient, which accounts for the mixture's ability to absorb radiative energy, was also amplified with increasing H_2O content—a trend very similar to that of optical thickness. Thus, these two factors should counter-balance each other and the direct radiative effect could not adequately explain the increment of radiation reabsorption effects with increasing H_2O content.

Moreover, the flame structures (of a fixed H_2O mole fraction in the inlet py-gas, 44%) calculated by ADI and SNB are presented in Fig. 7 to illustrate the preheat-induced chemical effect during radiation

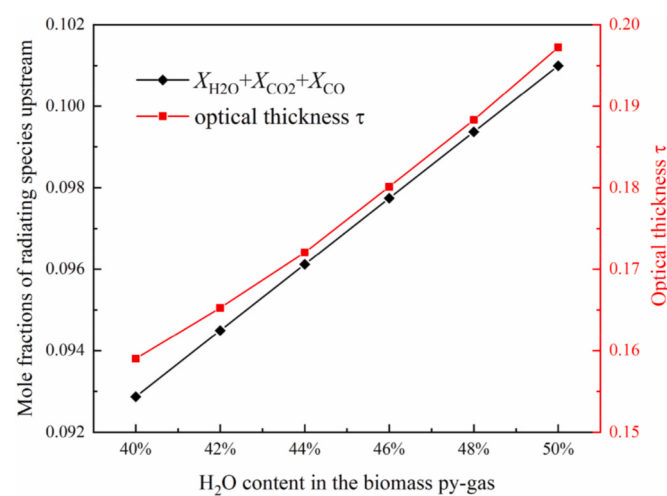


Fig. 6. The optical thickness and summed mole fraction of H_2O , CO_2 and CO in the upstream unburned region of py-gas/air mixtures with various H_2O contents ($P = 1$ atm and $T_{\text{in}} = 400$ K).

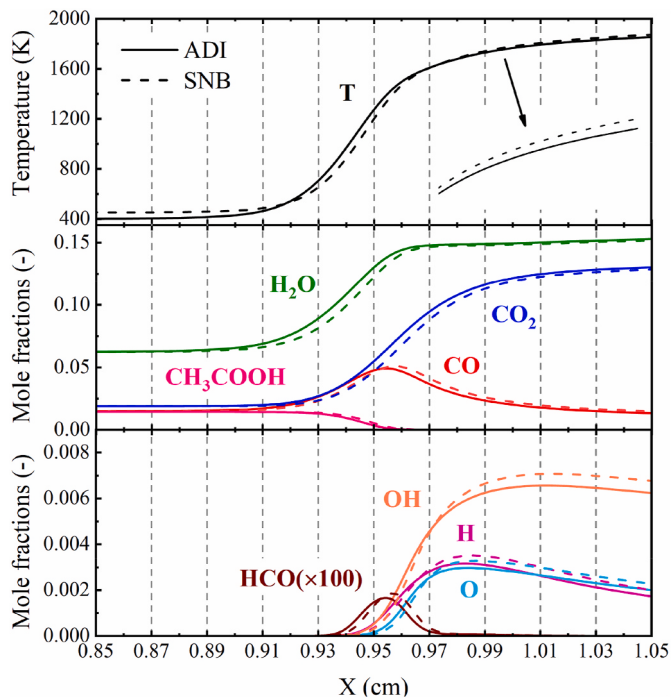


Fig. 7. Distributions of temperature, major species and radicals for a py-gas/air mixtures (44% vol. H_2O in the py-gas) calculated by ADI (solid lines) and SNB (dashed lines).

reabsorption. In comparison to mole fractions of major species, the mole fractions of radicals were more significantly affected by the radiation reabsorption effect (the peak concentrations of radicals differed by up to 11.81%). It could also be seen that, with the SNB model, temperature in the upstream unburned region that absorbed radiative energy from the downstream high-temperature region [45], was higher than that obtained with the ADI, and the concentrations of radicals were consequently elevated due to this preheat-induced chemical effect.

As the rate of production (ROP) results for H_2O shown in Fig. 8, with the two inlet temperatures ($T_{in} = 400 \text{ K}$ and 450 K) and 44% vol. H_2O in the py-gas, the preheat effect induced by radiation reabsorption in the SNB model affected the production and consumption pathway of H_2O , thereby affecting H , O and OH radicals [46]. On the one hand, the main consumption pathway of H_2O , reversed reaction $2\text{OH} = \text{H}_2\text{O} + \text{O}$, was inhibited by the elevated inlet temperature (the relative difference for ROP between two inlet temperatures was 4.01%, calculated via $(\text{ROP}_{450\text{K}} - \text{ROP}_{400\text{K}})/\text{ROP}_{400\text{K}}$), which reduced the consumption of O and increased the production of OH . Meanwhile, most of the reaction pathways for the conversion of OH to H_2O were reduced by the elevated inlet temperature (the relative decrease of ROP was 6.09% for $\text{HO}_2 + \text{OH}$

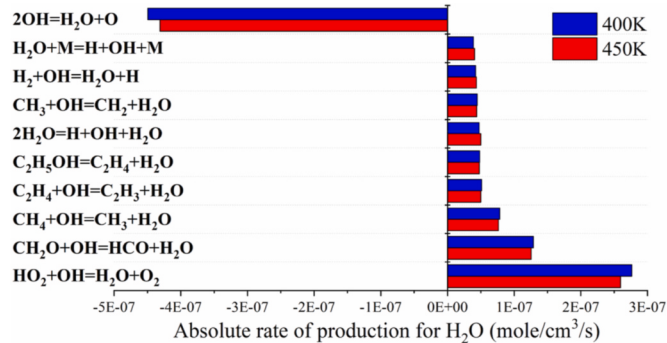


Fig. 8. Rates of production of H_2O for a py-gas/air mixtures (44% vol. H_2O in the py-gas) with two inlet temperatures ($T_{in} = 400 \text{ K}$ and 450 K , $P = 1 \text{ atm}$).

$= \text{H}_2\text{O} + \text{O}_2$, 2.48% for $\text{CH}_2\text{O} + \text{OH} = \text{HCO} + \text{H}_2\text{O}$, 2.34% for $\text{CH}_4 + \text{OH} = \text{CH}_3 + \text{H}_2\text{O}$, 2.39% for $\text{C}_2\text{H}_4 + \text{OH} = \text{C}_2\text{H}_3 + \text{H}_2\text{O}$ and 1.64% for $\text{CH}_3 + \text{OH} = \text{CH}_2 + \text{H}_2\text{O}$, respectively), indicating the consumption of OH was reduced in SNB. As for the H radical, at the same time when H generated more H_2O via $\text{H} + \text{OH} + \text{M} = \text{H} + \text{OH} + \text{M}$, the step $\text{H}_2 + \text{OH} = \text{H}_2\text{O} + \text{H}$ was promoted to produce more H due to the enhanced mole fraction of OH .

Fig. 9 shows the peak concentrations of the important radicals calculated by the two models with various H_2O contents and their relative differences caused by radiation reabsorption. As H_2O content increased, the relative differences of H , O , OH and HCO radicals all increased, with the maximum relative differences 18.02%, 15.52%, 11.48% and 18.11%, respectively. This indicated HCO radical was the most affected radical due to radiation reabsorption, although its concentration was much lower than H , OH and O . Meanwhile, as shown in Fig. 7, the peak location of HCO radical was more upstream than those of H , OH and O , suggesting these radicals could be affected by the change of HCO . Therefore, the role of HCO in the radiation reabsorption effect is further discussed next.

Since HCO was the most sensitive radical to radiation reabsorption effect, its sensitivity and ROP analyses were subsequently performed for mixtures with various H_2O contents. As shown in Fig. 10, $\text{HCO} + \text{M} = \text{H} + \text{CO} + \text{M}$ had the highest sensitivities and ROP results to HCO , among all the HCO -related reactions. However, its response to the change of H_2O content was much milder (and nearly neutral for the flame speed in Fig. 4) than the second sensitive HCO -consuming reaction $\text{HCO} + \text{O}_2 = \text{CO} + \text{HO}_2$, which was the most negative sensitive reaction of flame speed under high-water-content condition.

Furthermore, to examine the preheat effect induced by radiation reabsorption, the ROPs for the reactions $\text{HCO} + \text{O}_2 = \text{CO} + \text{HO}_2$ and $\text{HCO} + \text{M} = \text{H} + \text{CO} + \text{M}$ were calculated for two inlet temperatures (at $T_{in} = 400 \text{ K}$ and 450 K , respectively, see Fig. 11). It indicated that the elevated inlet temperature reduced the ROPs of these key reactions and hence inhibited the consumption of HCO radical. Characteristically, the relative differences of ROP for $\text{HCO} + \text{O}_2 = \text{CO} + \text{HO}_2$ with 40% and 50% H_2O content in the py-gas were 3.83% and 7.13%, respectively; such differences were consistently around 1.75% for $\text{HCO} + \text{M} = \text{H} + \text{CO} + \text{M}$. Hence, this preheat-induced inhibition effect (due to radiation reabsorption that heated the upstream) primarily acted on $\text{HCO} + \text{O}_2 = \text{CO} + \text{HO}_2$, which was monotonically strengthened with increasing H_2O content in the inlet py-gas. Consequently, the relative SNB-ADI differences of HCO radical shown in Fig. 9 increased with higher H_2O

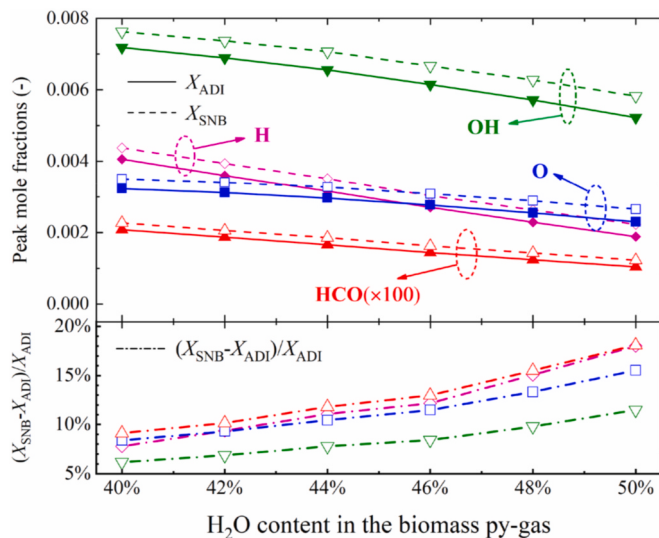


Fig. 9. The peak mole fractions and relative differences of O , H , OH and HCO radicals calculated by ADI and SNB for py-gas/air mixtures with various H_2O contents ($P = 1 \text{ atm}$ and $T_{in} = 400 \text{ K}$).

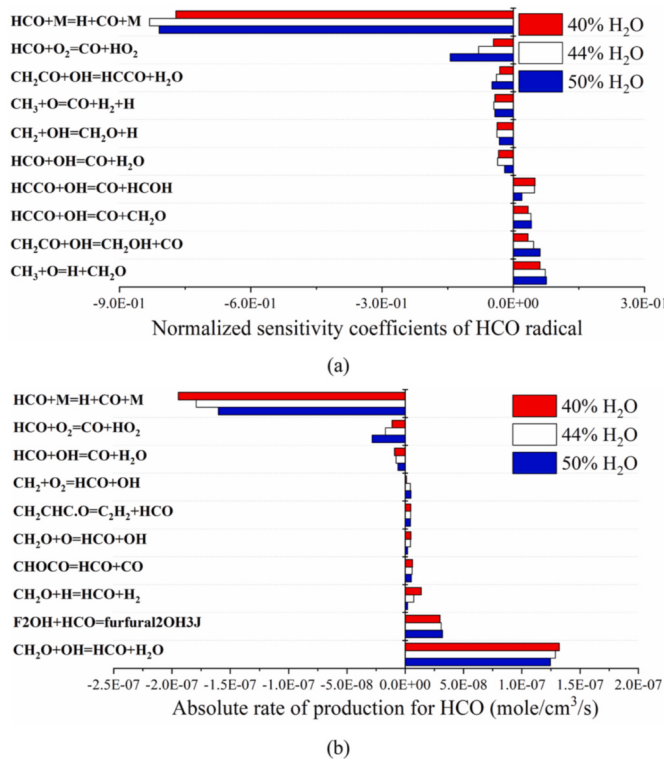


Fig. 10. (a) Normalized sensitivity coefficients and (b) absolute rates of production of HCO for py-gas/air mixtures with various H₂O contents ($P = 1$ atm and $T_{in} = 400$ K).

contents. Meanwhile, $\text{HCO} + \text{O}_2 = \text{CO} + \text{HO}_2$ was the most sensitive reaction decelerating the laminar flame speed, with larger sensitivity coefficient under higher H₂O content (Fig. 4). Evidently, the increased relative differences of laminar flame speeds R_s in Fig. 2 could be attributed to the increasing inhibition by the flame-speed-decelerating reaction $\text{HCO} + \text{O}_2 = \text{CO} + \text{HO}_2$.

3.2. Effects on NO emission

Fig. 12 shows the outlet mole fractions of NO calculated by ADI and SNB with various H₂O contents in the py-gas, along with their relative differences as a result of radiation reabsorption. The maximum NO emission obtained with ADI and SNB occurred in the 40%-H₂O case (386.4 and 334.0 ppm, respectively) and were both suppressed by increasing H₂O content (386.4–192.9 ppm for ADI and 334.0 to 190.6 ppm for SNB when H₂O content in the py-gas was increased to 50%). Comparisons between the two models indicated that NO emission became lower when radiation reabsorption was considered, with the maximum relative difference between SNB and ADI of 13.56% occurring in the lowest-H₂O case, which dropped to 1.20% in the highest-H₂O case.

To study the formation mechanism of NO during py-gas combustion, the related reaction pathway is shown in Fig. 13. Two nitrogen sources existed in the py-gas/air flame, namely nitrogen (N₂) in the air and pyridine (C₅H₅N) from the bio-oil. The formation of NO was mainly through three different routes: thermal-NO, prompt-NO and fuel-NO (marked with red, green and blue colors in Fig. 13, respectively). The thermal-NO and prompt-NO routes were both initiated from N₂. The former was mainly initiated by the high-temperature-sensitive above 1800 K, primarily involving the reactions $\text{N}_2 + \text{O} = \text{N} + \text{NO}$, $\text{N} + \text{OH} = \text{NO} + \text{H}$ and $\text{N} + \text{O}_2 = \text{NO} + \text{O}$. The latter was induced by the reactions between N₂ and CH_i radicals, whose main product was NCN radical. Subsequently, NCN radicals reacted with O atom and yielded CN, which was subsequently converted to NCO though the reaction $\text{HCN} + \text{O} =$

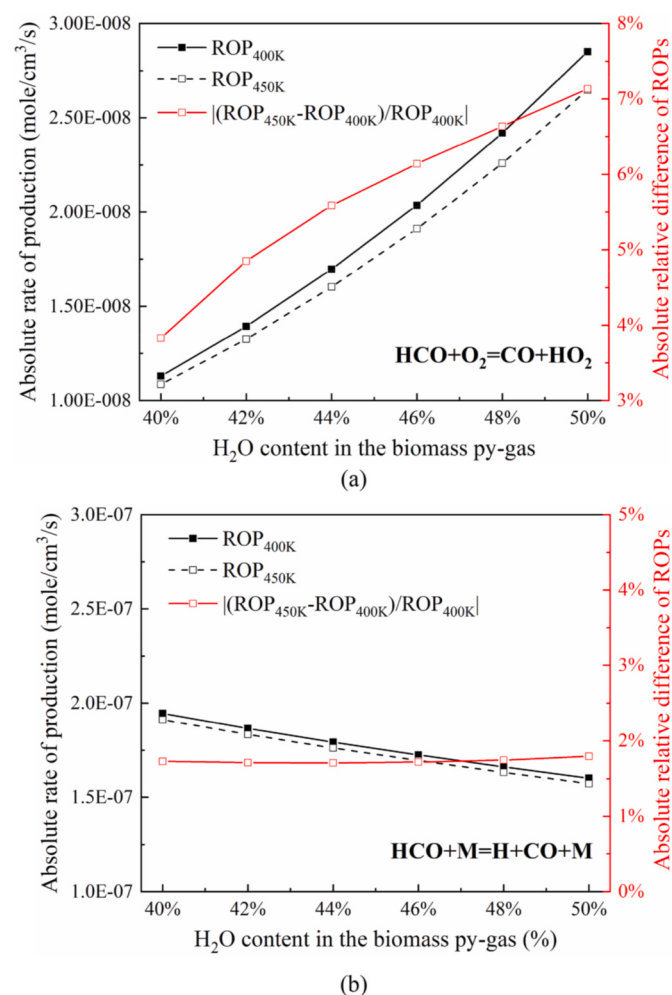


Fig. 11. Absolute ROP results and the relative differences of (a) $\text{HCO} + \text{O}_2 = \text{CO} + \text{HO}_2$ and (b) $\text{HCO} + \text{M} = \text{H} + \text{CO} + \text{M}$ with two inlet temperatures ($T_{in} = 400$ K and 450 K) for py-gas/air mixtures with various H₂O contents ($P = 1$ atm).

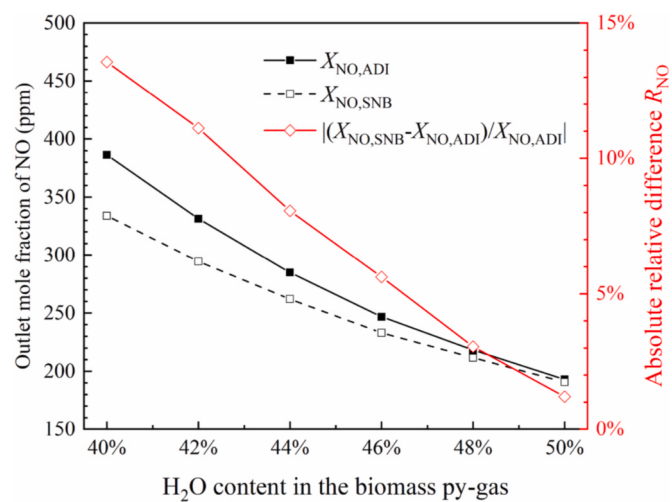


Fig. 12. Outlet NO mole fractions obtained by ADI and SNB models and their relative differences (i.e., effect of radiation reabsorption) for py-gas/air mixtures with various H₂O contents ($P = 1$ atm and $T_{in} = 400$ K).

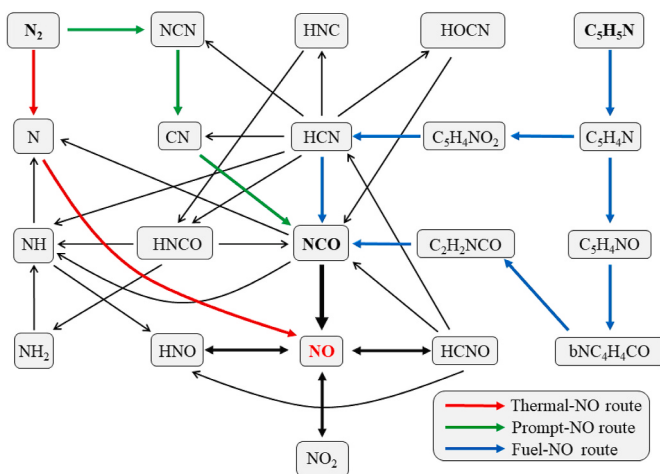


Fig. 13. Main reaction pathway of NO during the combustion of a py-gas/air mixture (44% vol. H₂O in the py-gas, $P = 1$ atm and $T_{in} = 400$ K). Reactions with relative ROP less than 5% were neglected.

NCO + H. As for the fuel-NO route, the branch started via the transformation of C₅H₄N (mainly the decomposition via C₅H₅N + OH = C₅H₄N + H₂O). Next, on the one hand, N was transferred from C₅H₄N to NCO through intermediates C₅H₄NO, bNC₄H₄CO and C₂H₂NCO. On the other hand, C₅H₄N was also converted to C₅H₄NO₂, which was then decomposed to CO and HCN. About 20% HCN was directly converted to NO via NCO, while the remaining indirectly ended in NO or NO₂ via NH/HNC/HNCO and some other species. In conclusion, NCO was the key intermediate radical in the NO formation process during py-gas combustion, involving in both prompt-NO and fuel-NO routes. This was consistent with previous study on pure pyridine oxidation [36].

ROP and sensitivity analyses of NO also confirmed the above discussion. As shown in Fig. 14, the reactions related to NO, NO₂ and HNO

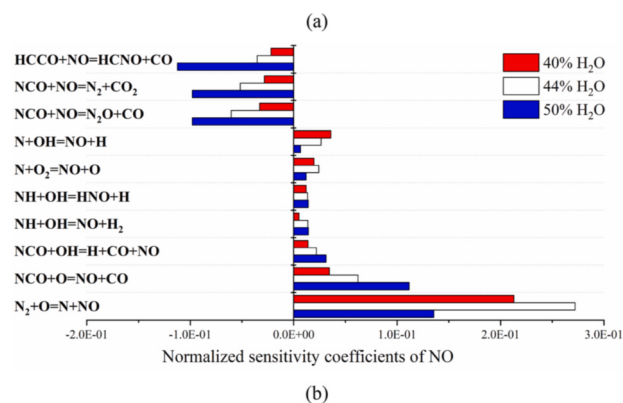
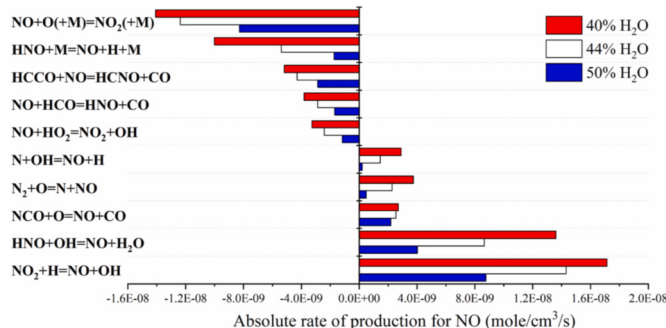


Fig. 14. (a) Absolute rates of production and (b) normalized sensitivity coefficients of NO for py-gas/air mixtures with various H₂O contents ($P = 1$ atm and $T_{in} = 400$ K).

had the larger ROPs for NO production; however, they were counterbalanced by their NO-consuming reactions. The sensitivity analysis also manifested that it is the thermal-NO route (N₂ + O = N + NO) and reactions associated with NCO (NCO + O = NO + CO and NCO + OH = H + CO + NO) that were the most sensitive steps for NO generation. As supported by the relative contributions of each radical to NO production shown in Fig. 15, the contributions of NO₂ and HNO were the largest, which were however, counterbalanced by their NO-consuming reactions. Even in the case of increasing H₂O content, the relative contributions of NO₂, HNO and HNCO route to NO production and destruction remained consistent. Eventually, it was the thermal and NCO routes that really determined the NO emission. With the increase of water content, the contribution of thermal-NO route gradually decreased and that of NCO surpassed it.

Finally, the outlet temperatures and the peak concentrations of NCO obtained with ADI and SNB models, and their relative differences R_T and R_{NCO} are provided in Figs. 16 and 17. Outlet temperature and peak mole fraction of NCO both decreased with rising H₂O content, indicating that the NO formation via thermal route and NCO route both decreased with increasing H₂O content, which is consistent with the overall tendency of NO emission against water content in Fig. 12. After considering the radiation reabsorption, the outlet temperature obtained via SNB was lower than that via ADI due to radiative heat loss, but meanwhile the SNB cases had larger NCO concentrations owing to radiation preheating effect. Thus, comparing to the ADI cases, the SNB cases had weaker thermal-route NO production and stronger NCO-route NO production, which resulted in overall less NO emission than the ADI cases. More H₂O suppressed the thermal-route (see Fig. 15 where NCO-route became relatively stronger) and hence the gas between ADI- and SNB-predicted NO emission vanished with increasing H₂O content in Fig. 12.

4. Conclusion

One-dimensional numerical simulations for premixed py-gas/air combustion were conducted at atmospheric pressure and with inlet gas temperature 400 K. Laminar flame speeds and NO emissions were calculated by using ADI and SNB models with various H₂O contents. The thermal and chemical effects of H₂O content, and especially the effect of radiation reabsorption, on laminar flame speed and NO emission were investigated via ROP and sensitivity analyses. The main findings could be concluded as follows.

- With increasing H₂O contents in the inlet py-gas, the laminar flame speed decreased as a result of combined dilutive, thermal and chemical effects. ROP analysis with various inlet H₂O contents revealed that increasing H₂O content consumed more O radicals via the step H₂O + O = 2OH, which further led to lower

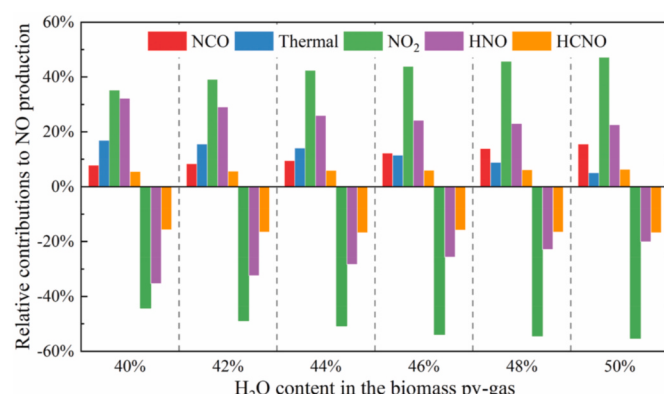


Fig. 15. Relative contribution to NO production of py-gas/air mixtures with various H₂O contents ($P = 1$ atm and $T_{in} = 400$ K), bars with positive value denote NO production and negative destruction).

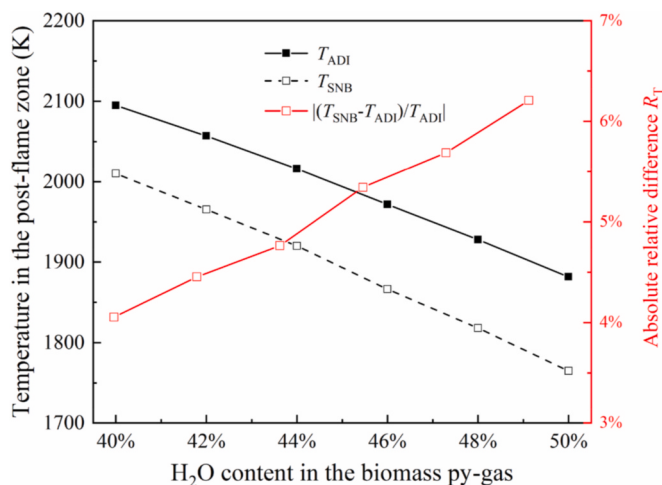


Fig. 16. Outlet temperatures (far downstream at $x = 20$ cm) and the relative differences between results obtained via ADI and SNB models for py-gas/air mixtures with various H₂O contents ($P = 1$ atm and $T_{in} = 400$ K).

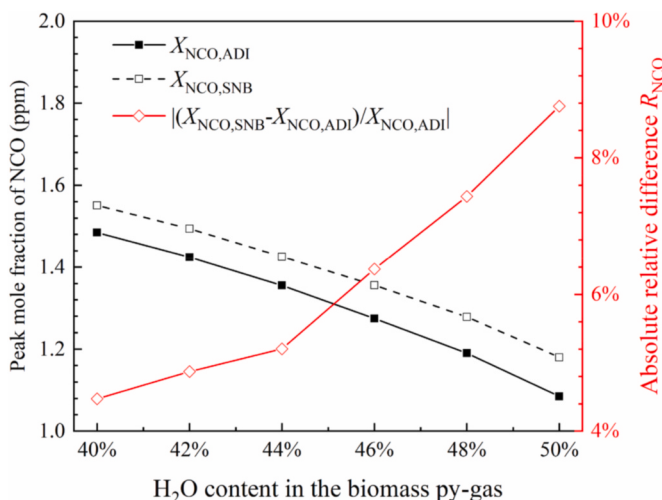


Fig. 17. Peak mole fractions of NCO (located at the reaction zone $x = \sim 0.95$ cm) and the relative differences between results obtained via ADI and SNB models for py-gas/air mixtures with various H₂O contents ($P = 1$ atm and $T_{in} = 400$ K).

- concentrations of H and OH (the latter through accelerated $\text{HO}_2 + \text{OH} = \text{H}_2\text{O} + \text{O}_2$), and consequently the laminar flame speed was decreased.
- (2) Discrepancies in laminar flame speeds predicted by the ADI and SNB models were due to the radiation reabsorption, whose effect increased from 9.92% to 17.42% when the H₂O content in the py-gas increased from 40% to 50%. Radiation reabsorption affected laminar flame speed mainly via a preheat-induced chemical effect. The preheat-induced inhibition on laminar flame speed, mainly via the dominant HCO-consumption reaction $\text{HCO} + \text{O}_2 = \text{CO} + \text{HO}_2$, resulted in larger discrepancies between the ADI and SNB results with rising H₂O content.
 - (3) NO formation primarily originated from thermal-NO and fuel-NO routes, related to temperature in the post-flame zone and concentrations of NCO radicals in the reaction zone, respectively. With increasing H₂O content, thermal-NO became weaker and fuel-NO (mainly through NCO) relatively stronger, resulting in a continuous decrement of NO emission and narrowing gap between the ADI and SNB predictions.

CRediT authorship contribution statement

Shu Zheng: Methodology, Formal analysis, Investigation, Conceptualization, Writing – original draft. **Hao Liu:** Writing – review & editing, Data curation. **Yuzhen He:** Software. **Yu Yang:** Formal analysis. **Ran Sui:** Supervision, Writing - review & editing. **Qiang Lu:** Supervision, Project administration.

Declaration of competing interest

The authors declare that they have no known competing financial interests or personal relationships that could have appeared to influence the work reported in this paper.

Data availability

Data will be made available on request.

Acknowledgements

This research was supported by the National Natural Science Foundation of China (Nos. 52276185, 52276189 and 52206157), the Fundamental Research Funds for the Central Universities (No. 2020JG005, 2020DF01). RS in addition acknowledges support from NSFC through a National Talent Program.

Appendix A. Supplementary data

Supplementary data to this article can be found online at <https://doi.org/10.1016/j.renene.2023.02.013>.

References

- [1] D.O. Glushkov, G.S. Nyashina, R. Anand, P.A. Strizhak, Composition of gas produced from the direct combustion and pyrolysis of biomass, Process Saf. Environ. Protect. 156 (2021) 43–56, <https://doi.org/10.1016/j.psep.2021.09.039>.
- [2] A.A. Bhuiyan, A.S. Blieblau, A.K.M.S. Islam, J. Naser, A review on thermo-chemical characteristics of coal/biomass co-firing in industrial furnace, J. Energy Inst. 91 (1) (2018) 1–18, <https://doi.org/10.1016/j.joei.2016.10.006>.
- [3] J.D. Morris, S.S. Daood, S. Chilton, W. Nimmo, Mechanisms and mitigation of agglomeration during fluidized bed combustion of biomass: a review, Fuel 230 (2018) 452–473, <https://doi.org/10.1016/j.fuel.2018.04.098>.
- [4] N.C. Cruz, F.C. Silva, L.A.C. Tarelho, S.M. Rodrigues, Critical review of key variables affecting potential recycling applications of ash produced at large-scale biomass combustion plants, Resour. Conserv. Recycl. 150 (2019), <https://doi.org/10.1016/j.resconrec.2019.104427>.
- [5] C. Liu, B. Yan, G. Chen, X.S. Bai, Structures and burning velocity of biomass derived gas flames, Int. J. Hydrogen Energy 35 (2) (2010) 542–555, <https://doi.org/10.1016/j.ijhydene.2009.11.020>.
- [6] H.-S. Do, T.-S. Tran, Z. Han, X. Zeng, S. Gao, G. Xu, Synergetic NO reduction by biomass pyrolysis products simulating their reburning in circulating fluidized bed decoupling combustion, Chin. J. Chem. Eng. 27 (7) (2019) 1680–1689, <https://doi.org/10.1016/j.cjche.2018.07.002>.
- [7] C. Wang, H. Ding, Y. Zhang, X. Zhu, Analysis of property variation and stability on the aging of bio-oil from fractional condensation, Renew. Energy 148 (2020) 720–728, <https://doi.org/10.1016/j.renene.2019.10.159>.
- [8] J. Xie, D. Su, X. Yin, C. Wu, J. Zhu, Thermodynamic analysis of aqueous phase reforming of three model compounds in bio-oil for hydrogen production, Int. J. Hydrogen Energy 36 (24) (2011) 15561–15572, <https://doi.org/10.1016/j.ijhydene.2011.08.103>.
- [9] T. Kulbeik, M. Scherzinger, I. Höfer, M. Kaltschmitt, Autoclave pre-treatment of foliage – effects of temperature, residence time and water content on solid biofuel properties, Renew. Energy 171 (2021) 275–286, <https://doi.org/10.1016/j.renene.2021.02.090>.
- [10] L. Burhenne, M. Damiani, T. Aicher, Effect of feedstock water content and pyrolysis temperature on the structure and reactivity of spruce wood char produced in fixed bed pyrolysis, Fuel 107 (2013) 836–847, <https://doi.org/10.1016/j.fuel.2013.01.033>.
- [11] R.J.M. Westerhof, N.J.M. Kuipers, S.R.A. Kersten, W.P.M. van Swaaij, Controlling the water content of biomass fast pyrolysis oil, Ind. Eng. Chem. Res. 46 (26) (2007) 9238–9247, <https://doi.org/10.1021/ie070684k>.
- [12] J. Shankar Tumuluru, C. T Wright, R. D Boardman, N.A. Yancey, S. Sokhansanj, A review on biomass classification and composition, co-firing issues and pretreatment methods, in: ASABE Annual Meeting, 2011, <https://doi.org/10.13031/2013.37191>.

- [13] S. Meng, S. Sun, H. Xu, Y. Guo, D. Feng, Y. Zhao, P. Wang, Y. Qin, The effects of water addition on the laminar flame speeds of CO/H₂/O₂/H₂O mixtures, Int. J. Hydrogen Energy 41 (25) (2016) 10976–10985, <https://doi.org/10.1016/j.ijhydene.2016.04.251>.
- [14] I.S. Anufriev, Review of water/steam addition in liquid-fuel combustion systems for NOx reduction: waste-to-energy trends, Renew. Sustain. Energy Rev. 138 (2021), <https://doi.org/10.1016/j.rser.2020.110665>.
- [15] N.F. Munajat, C. Erlich, R. Fakhrai, T.H. Fransson, Influence of water vapour and tar compound on laminar flame speed of gasified biomass gas, Appl. Energy 98 (2012) 114–121, <https://doi.org/10.1016/j.apenergy.2012.03.010>.
- [16] C.H. Sohn, Z. Chen, Y. Ju, Effects of radiation on the uncertainty of flame speed determination using spherically propagating flames with CO/CO₂/H₂O dilutions at elevated pressures, Int. J. Heat Mass Tran. 86 (2015) 820–825, <https://doi.org/10.1016/j.ijheatmasstransfer.2015.03.062>.
- [17] K. Yoshihaga, H. Kobayashi, Numerical study of radiation effects on polypropylene combustion using high-temperature oxidizer diluted with H₂O and CO₂, J. Therm. Sci. Technol. 3 (2) (2008) 167–178, <https://doi.org/10.1299/jst.3.167>.
- [18] J. Wang, T. Niioka, Numerical study of radiation reabsorption effect on NO_x formation in CH₄/air counterflow premixed flames, Proc. Combust. Inst. 29 (2) (2002) 2211–2217, [https://doi.org/10.1016/s1540-7489\(02\)80269-3](https://doi.org/10.1016/s1540-7489(02)80269-3).
- [19] C. Di Blasi, G. Signorelli, C. Di Russo, G. Rea, Product distribution from pyrolysis of wood and agricultural residues, Ind. Eng. Chem. Res. 38 (6) (1999) 2216–2224, <https://doi.org/10.1021/ie980711u>.
- [20] Y. Chhiti, M. Peyrot, S. Salvador, Soot formation and oxidation during bio-oil gasification: experiments and modeling, J. Energy Chem. 22 (5) (2013) 701–709, [https://doi.org/10.1016/s2095-4956\(13\)60093-5](https://doi.org/10.1016/s2095-4956(13)60093-5).
- [21] H. Li, Y. Yu, F. Yi, J. Qiang, C. Li, N. Zhao, J. Lu, Z. Jia, L. Zhou, P. Mperejekumana, H. Elshareef, Y. Zhou, R. Dong, Characteristics and formation of nitrogen-containing products from the pyrolysis of maple wood and maize straw, J. Anal. Appl. Pyrolysis 163 (2022), <https://doi.org/10.1016/j.jaap.2022.105462>.
- [22] B. Valle, A.G. Gayubo, A. Atutxa, A. Alonso, J. Bilbao, Integration of thermal treatment and catalytic transformation for upgrading biomass pyrolysis oil, Int. J. Chem. React. Eng. 5 (1) (2007), <https://doi.org/10.2202/1542-6580.1559>.
- [23] E. Vagia, A. Lemonidou, Thermodynamic analysis of hydrogen production via steam reforming of selected components of aqueous bio-oil fraction, Int. J. Hydrogen Energy 32 (2) (2007) 212–223, <https://doi.org/10.1016/j.ijhydene.2006.08.021>.
- [24] F. Lin, C.L. Waters, R.G. Mallinson, L.L. Lobban, L.E. Bartley, Relationships between biomass composition and liquid products formed via pyrolysis, Front. Energy Res. 3 (2015), <https://doi.org/10.3389/fenrg.2015.00045>.
- [25] Y. Liu, Q. Shi, Y. Zhang, Y. He, K.H. Chung, S. Zhao, C. Xu, Characterization of red pine pyrolysis bio-oil by gas chromatography-mass spectrometry and negative-ion electrospray ionization fourier transform ion cyclotron resonance mass spectrometry, Energy Fuel. 26 (7) (2012) 4532–4539, <https://doi.org/10.1021/ef300501t>.
- [26] S. Zheng, H. Liu, R. Sui, B. Zhou, Q. Lu, Effects of radiation reabsorption on laminar NH₃/H₂/air flames, Combust. Flame 235 (2022), <https://doi.org/10.1016/j.combustflame.2021.111699>.
- [27] S. Zheng, H. Liu, D. Li, Z. Liu, B. Zhou, Q. Lu, Effects of radiation reabsorption on the laminar burning velocity of methane/air and methane/hydrogen/air flames at elevated pressures, Fuel 311 (2022), <https://doi.org/10.1016/j.fuel.2021.122586>.
- [28] I.E. Gordon, L.S. Rothman, C. Hill, R.V. Kochanov, Y. Tan, P.F. Bernath, M. Birk, V. Boudon, A. Campargue, K.V. Chance, B.J. Drouin, J.M. Flaud, R.R. Gamache, J. T. Hodges, D. Jacquemart, V.I. Perevalov, A. Perrin, K.P. Shine, M.A.H. Smith, J. Tennyson, G.C. Toon, H. Tran, V.G. Tyuterev, A. Barbe, A.G. Császár, V.M. Devi, T. Furtenbacher, J.J. Harrison, J.M. Hartmann, A. Jolly, T.J. Johnson, T. Karman, I. Kleiner, A.A. Kyuberis, J. Loos, O.M. Lyulin, S.T. Massie, S.N. Mikhailenko, N. Moazzen-Ahmadi, H.S.P. Müller, O.V. Naumenko, A.V. Nikitin, O.L. Polyansky, M. Rey, M. Rotger, S.W. Sharpe, K. Sung, E. Starikova, S.A. Tashkun, J.V. Auwera, G. Wagner, J. Wilzewski, P. Wcislo, S. Yu, E.J. Zak, The HITRAN2016 molecular spectroscopic database, J. Quant. Spectrosc. Radiat. Transfer 203 (2017) 3–69, <https://doi.org/10.1016/j.jqsrt.2017.06.038>.
- [29] S. Zheng, Y. He, B. Hu, J. Zhu, B. Zhou, Q. Lu, Effects of radiation reabsorption on the flame speed and NO emission of NH₃/H₂/air flames at various hydrogen ratios, Fuel 327 (2022), <https://doi.org/10.1016/j.fuel.2022.125176>.
- [30] R.J. Kee, J.F. Grcar, M.D. Smooke, J.A. Miller, E. Meeks, PREMIX: A FORTRAN Program for Modeling Steady Laminar One-Dimensional Premixed Flames, 1985.
- [31] M. Christensen, A.A. Konnov, Laminar burning velocity of acetic acid + air flames, Combust. Flame 170 (2016) 12–29, <https://doi.org/10.1016/j.combustflame.2016.05.007>.
- [32] Y. Chang, M. Jia, Y. Li, Y. Liu, M. Xie, H. Wang, R.D. Reitz, Development of a skeletal mechanism for diesel surrogate fuel by using a decoupling methodology, Combust. Flame 162 (10) (2015) 3785–3802, <https://doi.org/10.1016/j.combustflame.2015.07.016>.
- [33] Z.-H. Jin, D. Yu, Y.-X. Liu, Z.-Y. Tian, S. Richter, M. Braun-Unkhoff, C. Naumann, J.-Z. Yang, An experimental investigation of furfural oxidation and the development of a comprehensive combustion model, Combust. Flame 226 (2021) 200–210, <https://doi.org/10.1016/j.combustflame.2020.12.015>.
- [34] M. Pelucchi, C. Cavallotti, A. Cuoci, T. Faravelli, A. Frassoldati, E. Ranzi, Detailed kinetics of substituted phenolic species in pyrolysis bio-oils, React. Chem. Eng. 4 (3) (2019) 490–506, <https://doi.org/10.1039/c8re00198g>.
- [35] N. Lamoureux, H.E. Merhubi, L. Pillier, S. de Persis, P. Desgroux, Modeling of NO formation in low pressure premixed flames, Combust. Flame 163 (2016) 557–575, <https://doi.org/10.1016/j.combustflame.2015.11.007>.
- [36] L.-N. Wu, Z.-Y. Tian, K.-R. Jin, Z.-H. Zheng, D. Wang, B.-Z. Liu, Q. Xu, Z.-D. Wang, Experimental and kinetic study of pyridine oxidation under the fuel-lean condition in a jet-stirred reactor, Combust. Flame (2022), <https://doi.org/10.1016/j.combustflame.2022.112042>.
- [37] S.Y. Liao, D.M. Jiang, Q. Cheng, Determination of laminar burning velocities for natural gas, Fuel 83 (9) (2004) 1247–1250, <https://doi.org/10.1016/j.fuel.2003.12.001>.
- [38] C. Ji, R. Zhao, B. Li, F.N. Egolfopoulos, Propagation and extinction of cyclopentadiene flames, Proc. Combust. Inst. 34 (1) (2013) 787–794, <https://doi.org/10.1016/j.proci.2012.07.047>.
- [39] A. Katoch, A. Millán-Merino, S. Kumar, Measurement of laminar burning velocity of ethanol-air mixtures at elevated temperatures, Fuel 231 (2018) 37–44, <https://doi.org/10.1016/j.fuel.2018.05.083>.
- [40] X. Zhang, B. Mei, S. Ma, Y. Zhang, C. Cao, W. Li, L. Ye, Y. Li, Characterizing the fuel-specific combustion chemistry of acetic acid and propanoic acid: laminar flame propagation and kinetic modeling studies, Proc. Combust. Inst. 38 (1) (2021) 449–457, <https://doi.org/10.1016/j.proci.2020.06.220>.
- [41] M.U. Alzueta, A. Tena, R. Bilbao, Pyridine conversion in a flow reactor and its interaction with nitric oxide, Combust. Sci. Technol. 174 (10) (2002) 151–169, <https://doi.org/10.1080/00102200290021470>.
- [42] E.C. Okafor, Y. Naito, S. Colson, A. Ichikawa, T. Kudo, A. Hayakawa, H. Kobayashi, Experimental and numerical study of the laminar burning velocity of CH₄-NH₃-air premixed flames, Combust. Flame 187 (2018) 185–198, <https://doi.org/10.1016/j.combustflame.2017.09.002>.
- [43] P. Xiao, C.-F. Lee, H. Wu, F. Liu, Effects of hydrogen addition on the laminar methanol-air flame under different initial temperatures, Renew. Energy 154 (2020) 209–222, <https://doi.org/10.1016/j.renene.2020.03.037>.
- [44] Y. Ju, G. Masuya, P.D. Ronney, Effects of radiative emission and absorption on the propagation and extinction of premixed gas flames, Symp. (Int.) Combust. 27 (2) (1998) 2619–2626, [https://doi.org/10.1016/s0082-0784\(98\)80116-1](https://doi.org/10.1016/s0082-0784(98)80116-1).
- [45] S. Zheng, R. Sui, W. Liang, H. Zhou, C.K. Law, On band lumping, radiation reabsorption, and high-pressure effects in laminar flame propagation, Combust. Flame 221 (2020) 86–93, <https://doi.org/10.1016/j.combustflame.2020.07.042>.
- [46] R. Sui, W. Liang, L. Zhang, J. Mantzaras, C.K. Law, Kinetic interactions between H₂ and CO in catalytic oxidation over PdO, Combust. Flame 211 (2020) 270–280, <https://doi.org/10.1016/j.combustflame.2019.09.035>.